Published in final edited form as:
*Cancer Res.* 2012 July 1; 72(13): 3381–3392. doi:10.1158/0008-5472.CAN-11-3525.

# Definition of Genetic Events Directing the Development of Distinct Types of Brain Tumors from Postnatal Neural Stem/ Progenitor Cells

**Falk Hertwig**[2,4], **Katharina Meyer**[5], **Sebastian Braun**[2], **Sara Ek**[1], **Rainer Spang**[5], **Cosima V. Pfenninger**[2], **Isabella Artner**[2], **Gaëlle Prost**[2], **Xinbin Chen**[6], **Jaclyn A. Biegel**[7], **Alexander R. Judkins**[8], **Elisabet Englund**[3], and **Ulrike A. Nuber**[2]

[1]Department of Immunotechnology, Lund University Hospital, Lund, Sweden

[2]Lund Strategic Research Center for Stem Cell Biology, Department of Laboratory Medicine, Lund University, Lund University Hospital, Lund, Sweden

[3]Division of Neuropathology, Department of Pathology and Cytology, Lund University Hospital, Lund, Sweden

[4]Department of Biology, Chemistry and Pharmacy, Freie Universität Berlin

[5]Institute for Functional Genomics, University of Regensburg, Regensburg, Germany

[6]Center for Comparative Oncology, University of California, Davis, California

[7]Department of Pathology and Laboratory Medicine, The Children's Hospital of Philadelphia, Pennsylvania

[8]Department of Pathology and Laboratory Medicine, Children's Hospital Los Angeles, Keck School of Medicine, University of Southern California, Los Angeles, California

## Abstract

Although brain tumors are classified and treated based upon their histology, the molecular factors involved in the development of various tumor types remain unknown. In this study, we show that the type and order of genetic events directs the development of gliomas, central nervous system primitive neuroectodermal tumors, and atypical teratoid/rhabdoid-like tumors from postnatal



**Corresponding Author:** Ulrike A. Nuber, Lund Strategic Research Center for Stem Cell Biology, Department of Laboratory Medicine, Lund University, BMC B10, Klinikgatan 26, 221 84 Lund, Sweden. Phone: 46-46-222-1563; Fax: 46-46-222-3600; ulrike.nuber@med.lu.se.

**Note:** Supplementary data for this article are available at Cancer Research Online (http://cancerres.aacrjournals.org/).

**Disclosure of Potential Conflicts of Interest**
A patent has been filed (owner: U.A. Nuber). No potential conflicts of interest were disclosed by the other authors.

**Authors' Contributions**
**Conception and design:** F. Hertwig, U.A. Nuber
**Development of methodology:** F. Hertwig, S. Braun, C.V. Pfenninger, G. Prost, U.A. Nuber
**Acquisition of data (provided animals, acquired and managed patients, provided facilities, etc.):** F. Hertwig, S. Braun, G. Prost, X. Chen, E. Englund, U. A. Nuber
**Analysis and interpretation of data (e.g., statistical analysis, biostatistics, computational analysis):** F. Hertwig, K. Meyer, S. Braun, R. Spang, J.A Biegel, A. R. Judkins, E. Englund, U.A. Nuber
**Writing, review, and/or revision of the manuscript:** F. Hertwig, K. Meyer, S. Braun, S. Ek, R. Spang, I. Artner, J.A Biegel, A.R. Judkins, E. Englund, U.A. Nuber
**Administrative, technical, or material support (i.e., reporting or organizing data, constructing databases):** F. Hertwig, S. Ek, C.V. Pfenninger, I. Artner, U.A. Nuber
**Study supervision:** U.A. Nuber

mouse neural stem/progenitor cells (NSC/NPC). We found that the overexpression of specific genes led to the development of these three different brain tumors from NSC/NPCs, and manipulation of the order of genetic events was able to convert one established tumor type into another. In addition, loss of the nuclear chromatin-remodeling factor SMARCB1 in rhabdoid tumors led to increased phosphorylation of eIF2α, a central cytoplasmic unfolded protein response (UPR) component, suggesting a role for the UPR in these tumors. Consistent with this, application of the proteasome inhibitor bortezomib led to an increase in apoptosis of human cells with reduced SMARCB1 levels. Taken together, our findings indicate that the order of genetic events determines the phenotypes of brain tumors derived from a common precursor cell pool, and suggest that the UPR may represent a therapeutic target in atypical teratoid/rhabdoid tumors.



## Introduction

The pathologic classification of brain tumors is largely based on their histology, and treatment strategies still depend primarily on this classification. How different cells of origin, cell-intrinsic, and cell-extrinsic factors contribute to the development of distinct brain tumor types remains unclear. Today, 2 main models explain intertumoral heterogeneity: The cell-of-origin model according to which the various tumor types arise from different cells and the genetic mutation model that describes the occurrence of different mutations within the same cell-of-origin leading to diverse tumor types (1). Histologically, very similar murine brain tumor types [central nervous system (CNS) primitive neuroectodermal tumors (PNET) and medulloblastomas] can develop from different neural stem/progenitor cells (NSC/NPC; refs. 2–6). Alternatively, different mouse brain tumors can originate from common cells of origin that acquire divergent phenotypes. This is exemplified by CNS PNET and astrocytoma, which can arise from forebrain NSC/NPCs (3, 7–11). Whether the mere accumulation or the order of single genetic events determines tumor phenotypes and to which extent established tumor types are stable or can be converted into other distinct types remains unknown. Here we show that (i) the overexpression of specific genes leads to the development of 3 different brain tumors from postnatal lateral ventricle wall (LVW) NSC/NPCs, (ii) an established *in vivo* tumor type can be converted into another one, and (iii) this conversion is controlled by the order of genetic events. One of the tumor types resembles atypical teratoid/rhabdoid tumor (AT/RT), and we present a so far unrecognized involvement of the unfolded protein response (UPR) in AT/RTs and in malignant rhabdoid tumors (MRT) lacking *SMARCB1*. This gene encodes the SMARCB1 protein (also described as SNF5/INI1/BAF47), primarily known for its nuclear chromatin remodeling and gene regulation function (12). Biallelic *SMARCB1* inactivation is found in the vast majority of AT/RTs and MRTs, and reduced or lost *SMARCB1* expression has also been reported for other tumors (13–15). We show that reduced or absent SMARCB1 protein levels result in an elevated sensitivity toward eIF2α phosphorylation and lead to increased apoptosis upon treatment with a proteasome inhibitor.

## Materials and Methods

For detailed information see Supplementary Materials and Methods.

### Animals

C57Bl/6J and p53 knockout mice (TSG-p53) were from Taconic Europe. Transplantations into the right frontal brain lobe of 4- to 8-week-old C57Bl/6J mice were carried out.

### Neurosphere and tumorsphere culture

LVW tissue from 4-week-old mice and brain tumor tissue was dissected, digested with Accutase (PAA), and filtrated. Cells were fluorescence-activated cell sorting (FACS)-isolated based on eGFP and DsRed expression and cultured as spheres in Dulbecco's Modified Eagle's Medium/F12 (1:1) with Glutamax, B27, penicillin (100 units/mL), streptomycin (100 μg/mL; all from Invitrogen), HEPES (10 mmol/L), Partricin (0.5 μg/mL; Biochrom), insulin (20 μg/mL; Sigma Aldrich), EGF (20 ng/mL), and rhFGFbasic (20 ng/mL; PAN Biotech). Cells were passaged 5 to 7 days after plating.

### Viral transduction

The pCMMP-IRES2-eGFP retroviral vector was provided by Laurent Roybon (Lund University, Lund, Sweden). A DsRed vector was generated by replacing the IRES-eGFP sequence with IRES-DsRedExpress. Human *MYC*, human *V12HRAS*, mouse *Bmi1*, mouse *Ezh2*, and mouse *FoxM1* cDNA sequences were inserted upstream of the IRES sequences. EcoPack2-293 cells (BD Biosciences) were used to produce viral supernatant.

### FACS

Tissue or cells were dissociated (see above), washed twice in PBS/1% bovine serum albumin, and 7-AAD (Sigma/Merck) was added for dead cell discrimination. A FACSVantage system (DiVa option; BD Biosciences) was used and doublets and dead cells were excluded. Sorted cells were centrifuged (5 minutes 200 *g*) and resuspended in growth medium. Cells were cultured at 37°C/5% $CO_2$ overnight or longer before transplantations.

### Immunostainings

Tissue was fixed (4% formaldehyde/PBS overnight) and either dehydrated and paraffin embedded or cryoprotected (25% sucrose/PBS) and embedded in TissueTek OCT compound (Sakura). Cells on coverslips were fixed with 4% formaldehyde/PBS for 10 minutes at room temperature. Immunostainings are described in the Supplementary Materials and Methods.

### Reverse transcriptase PCR

RNA was isolated (AllPrep DNA/RNA Mini Kit, Qiagen) and 2 μg was used for cDNA synthesis.

### Microarray hybridization and analysis

RNA was analyzed on the Agilent 2100 Bioanalyzer (Agilent Technologies). Sample generation, hybridization to Affymetrix Gene 1.0 ST Arrays, washing, and scanning were carried out according to the GeneChip Whole Transcript Sense Target Labeling Assay User manual, P/N 701880 Rev.5. 300 ng RNA was used for the first strand cDNA synthesis. Data were normalized by the Robust Multi-array Average method (Expression Console software) and are deposited at the gene expression omnibus database GEO (GSE28095). Gene set enrichment analysis (GSEA) was carried out per Subramanian and colleagues (16). Gene sets are listed in Supplementary File S1. Genes representing the different tumor types were found by correlating the 5,000 most variable genes across all samples to tumor type labels. To see whether the 1,000 highest ranked genes were differentially expressed between tumor types a linear model was fitted using the R package limma. All 1,000 genes showed a *P* value smaller than $10^{-6}$ and were considered for further analysis.

Complete linkage hierarchical clustering of tumorsphere samples was carried out based on Euclidean distances. For supervised classification we used shrunken centroid classification (R package PAMr).

### Western blot analysis

See Supplementary Materials and Methods. Antibodies: anti-BAF47 (SMARCB1/SNF5; BD Biosciences), anti-phospho-eIF2α (119A11; Cell Signaling), anti-β actin-HRP (Abcam).

### Cell lines

LM [ref. 15; obtained from R. Handgretinger (Universitätsklinikum Tübingen, Kinderheilkunde I, Tübingen, Germany) in 2010], CHLA-02-ATRT, A-204, and G401 (ref. 17; obtained from American Type Culture Collection in 2010), SW1783 and Hs683 (provided by M. Simon, Universitätsklinikum Bonn, Bonn, Germany, in 2008), 786-O, and A-498 (provided by A. Toelle, Charité - Universitätsmedizin Berlin, Klinik für Urologie, Berlin, Germany, in 2010), DAOY and BT12 (provided by M. Grotzer, University Children's Hospital Zurich, Dept. of Oncology, Zürich, Switzerland, in 2009 and 2010, respectively), HepG2 (obtained from P. Nilsson-Ehle, Lund University, Department of Laboratory Medicine, Lund, Sweden, in 2010), and MCF7 (obtained from X. Chen, Center for Comparative Oncology, University of California, Davis, CA, in 2010) cells were authenticated by morphology and SMARCB1 immunoblotting and kept without further authentication according to the Supplementary Materials and Methods.

## Results

### Lack of p53 and overexpression of multiple genes leads to oncogenic transformation of postnatal NSC/NPCs

Genetic perturbations were conducted to identify genes that lead to the oncogenic transformation of postnatal murine NSC/NPCs. Five genes [*Bmi1*, *Ezh2*, *FoxM1*, V12 mutant of *HRAS* in the following abbreviated as *HRAS*, and *MYC* (*c-MYC*); designated as mix] were simultaneously introduced by retroviral infections into wild-type (wt) or p53-deficient NSC/NPCs from the LVW of postnatal mice and passaged once as neurospheres. We chose these genes based on their role in neural stem cell maintenance, brain tumor development, or increased expression in brain tumors (18–23). The vectors contained the cDNA sequence of 1 of the 5 genes followed by an IRES-eGFP sequence, allowing us to isolate genetically altered cells by FACS. Because retroviral vectors only transduce dividing cells, we conclude that dividing NSC/NPCs were targeted. Tumors developed in all animals transplanted with 5,000 or more mix $p53^{-/-}$ cells, but not in mice that received any number of mix wt, empty $p53^{-/-}$ or empty wt cells (Supplementary Fig. S1A). Secondary and tertiary transplantations were carried out with FACS-isolated tumor cells and exogenous *MYC* and *HRAS* were found expressed in 8 investigated tumor samples, *Bmi1* and *Ezh2* in 4 and *FoxM1* in 3 cases (Supplementary Fig. S1B).

### *HRAS* or *MYC*, but not *Bmi1* or *Ezh2* overexpression in $p53^{-/-}$ postnatal NSC/NPCs generates tumor-initiating cells

To test the contribution of the individual genes to the development of brain tumors and to investigate which tumor types develop, we next conducted a combinatorial gene perturbation study, using cells from $p53^{-/-}$ mice and including *MYC*, *HRAS*, *Bmi1*, and *Ezh2* (Fig. 1A). *HRAS*-DsRed or *MYC*-DsRed viral vectors were used in combination with vectors for the expression of a second gene together with eGFP. FACS-isolated cells were transplanted into recipient mice (Fig. 1A). No tumors were observed in animals that received empty vector control cells or cells overexpressing *Bmi1* or *Ezh2* alone. Tumors developed in all animals transplanted with cells overexpressing *MYC* alone, or in combination with *HRAS*, *Bmi1*, or *Ezh2*, as well as in animals that received *HRAS* and *Bmi1* overexpressing cells. Tumors were furthermore detected in 2 of 3 animals transplanted with cells transduced with *HRAS* alone or *HRAS* plus *Ezh2*.

To assay the *in vivo* self-renewal capacity and stability of tumor types, we carried out serial transplantations with FACS-isolated tumor cells (Fig. 1A). These experiments revealed a high frequency of cells with tumor-forming capacity. In brain tumors that developed from all 7 tumorigenic gene combinations, including secondary tumor specimens of all but one gene combination (*HRAS* + *Ezh2*), DsRed and eGFP fluorescence was detected, albeit at different levels (Fig. 1B–D and data not shown).

## Overexpression of *HRAS* or *MYC* alone or in combination leads to the development of three brain tumor types from p53$^{-/-}$ postnatal NSC/NPCs

Three histologically different tumor types developed: PNETs, high-grade gliomas, and pleomorphic epithelioid tumors with abundant giant rhabdoid cells, which we refer to as AT/RT-like (Fig. 2 and Supplementary Fig. S2). All gliomas developed from cells with 3 different genetic perturbations: *HRAS* + *Bmi1*, *HRAS* + *Ezh2*, or *HRAS* alone. The PNETs developed from cells overexpressing *MYC* + *Bmi1*, *MYC* + *Ezh2*, and *MYC* alone. Interestingly, all AT/RT-like tumors developed from cells that overexpressed *HRAS* and *MYC* together, a combination of 2 oncogenes, which alone determined each of the other types, glioma (*HRAS*) or PNET (*MYC*). Cells from all 3 tumor types showed a high sphere formation rate *in vitro* (Supplementary Fig. S3); *in vivo*, AT/RT-like tumors developed faster than the other 2 (Fig. 1E). The general histologic features of the tumors remained stable throughout serial transplantations. The 3 tumor types also differed in their immunophenotypes (Fig. 3A and left panels in Supplementary Fig. S4A–D). Our finding of tenascin-C–positive glioma cells is in accordance with the reported localization of this protein. Tenascin-C is typically found at blood vessels of tumor tissues, and pericytes have been suggested as cellular source for this deposition (24). In high-grade glioma, however, it is also detected in the tumor cell cytoplasm and between tumor cells, indicating that tumor cells themselves synthesize tenascin-C in this malignancy (24, 25). No GFAP-positive glioma cells were found, and few tumor cells in some of the PNET and AT/RT-like samples showed GFAP staining. However the cells from which these tumors originated, p53$^{-/-}$ postnatal NSC/NPCs, were initially GFAP-positive (Fig. 3B). A progressive loss of GFAP can occur with increasing glioma grade and epigenetic silencing has been reported as one cause for this loss (26). We concluded that different genetic perturbations of murine postnatal NSC/NPCs from the LVW lead to the development of 3 malignant brain tumor types, which best correspond to high-grade glioma, CNS PNET (considering the forebrain origin of the NSC/NPCs and the forebrain transplantation site), and an AT/RT-like tumor. This histologic classification is supported by GSEA (see below).

## The three tumor cell types display distinct molecular signatures

Analysis of microarray gene expression data from 26 tumorsphere samples (developed under neurosphere culture conditions from FACS-isolated brain tumor cells; Supplementary Table S1) revealed a clustering into groups corresponding to the histologic classification (Fig. 4A). A shrunken centroid classifier (27) trained on truncated profiles predicted all tumor types correctly in cross-validation. Seven signature genes were sufficient for an error-free prediction of tumor types (Fig. 4B and C). Because the product of one of these genes (*Spp1*) has been suggested as diagnostic marker to distinguish AT/RTs from medulloblastoma (28) and as glioma grade indicator (29), we tested its expression at the protein level. Immunostainings confirmed the differential *Spp1* expression (table in Fig. 3, Fig. 4D, and left panels in Supplementary Fig. S4A–D). Although 7 genes were sufficient for tumor classification, many more genes showed differential expression in one of the tumor types relative to the 2 others (Fig. 5A and Supplementary Table S2). Differential gene expression data were analyzed for molecular expression signatures of human brain tumors by GSEA. Enrichment of human gene sets in the murine expression data is shown by high, normalized enrichment scores (NES; Fig. 5B), indicating that the generated murine tumors share key

expression signatures with respective human brain tumors. Thus, GSEA provided molecular support for our histologic classification.

## The *MYC*-induced CNS PNET phenotype is unstable and can be converted into an AT/RT-like tumor

We next asked how stable an established tumor phenotype is and whether it can be converted into another type by a consecutive genetic perturbation. Transplantion of $p53^{-/-}$ NSC/NPCs overexpressing *HRAS-DsRed* or *MYC-eGFP* generated gliomas and CNS PNETs. Cells from 2 gliomas and 2 CNS PNETs were FACS isolated. The glioma tumor cells were then transduced with *MYC-eGFP* viral vectors and the CNS PNET cells with *HRAS-DsRed* vectors. Sorted double positive cells were transplanted into recipient mice. The glioma daughter tumors retained most of their original features, except for the loss of tenascin-C in daughter tumors derived from 1 of the 2 gliomas (Supplementary Fig. S4A and B), whereas the CNS PNETs were converted into AT/RT-like types (Supplementary Fig. S4C and D). These CNS PNET daughter tumors consisted of cells with rhabdoid morphology, were positive for markers of the AT/RT-like tumors (vimentin, cytokeratin, and SPP1), and lost the ELAVL3/4 marker (characteristic for the CNS PNET mother tumors). Microarray profiles of FACS-purified tumorsphere cells from 2 mother and 4 daughter tumors (Supplementary Table S1) were determined. Our 7-gene tumor classifier assigned the glioma daughter tumors to the glioma profiles, whereas the CNS PNET daughter tumors were assigned to the AT/RT-like group (Fig. 6A). In summary, our histologic and gene expression data not only indicated that certain *in vivo* tumor phenotypes are plastic and can be changed by additional genetic events but also that the order of genetic events (overexpression of *HRAS* followed by *MYC* or *MYC* followed by *HRAS*) leads to the development of different *in vivo* tumor types (Fig. 6B).

## Genes related to the UPR are part of the AT/RT-like gene expression profile

Classical human AT/RTs are characterized by *SMARCB1* loss-of-function. In our AT/RT-like samples, however, no reduced *Smarcb1* mRNA levels were found, and SMARCB1 protein was detected in AT/RT-like tumors (Supplementary Fig. S5). To gain a better understanding of the molecular mechanisms leading to this phenotype, we took a look at the genes of group A (Fig. 5A), which were more highly expressed in AT/RT-like cells in comparison with CNS PNET and glioma cells. Whole Genome rVISTA analysis of transcription factor binding sites (30) located in 2,500 bp upstream regions of group A genes indicated only one overrepresented conserved motif ($P < 0.005$; Supplementary Table S3). This motif was originally named after a binding site of the transcription factor NF-E2, but later found to be recognized by other Cap "n" collar (CNC) family transcription factors (NRF1–3, BACH1–2; ref. 31). Several group A genes are known targets of a CNC protein that binds to NFE2 motifs, NRF2 (= NFE2L2), and of NF-κB (Supplementary Table S3). Both transcription factors are effector components of a pathway called the UPR (32), which is activated when the amount of unfolded proteins in the endoplasmic reticulum exceeds its folding capacity (also called endoplasmic reticulum stress). Endoplasmic reticulum stress pathways can be divided into 3 branches (PERK-eIF2α, ATF6, and IRE-XBP1) whose downstream consequences lead to cellular adaptation or death. Altogether, 43 of 134 group A genes (32.1%), which were more highly expressed in the AT/RT-like tumors, were identified as ER stress related (Supplementary Table S3). The analysis of genes previously found upregulated in human AT/RT and also upregulated in mouse embryonic fibroblasts upon deletion of the atypical teratoid/rhabdoid tumor suppressor gene *Smarcb1* (33) revealed that 35 of these 114 genes (30.7%) are related to endoplasmic reticulum stress (Supplementary Table S4).

### Loss of SMARCB1 results in an elevated sensitivity toward eIF2α phosphorylation

An involvement of the UPR in AT/RT biology has not been reported so far. Using an MCF7 breast cancer cell line, in which *SMARCB1* knockdown can be induced (34), we detected an increased phosphorylation of eIF2α upon SMARCB1 reduction (Fig. 7A). EIF2α is a central component of one UPR branch and can be phosphorylated by 4 different kinases (Fig. 7B). Dephosphorylation of eIF2α is carried out by the catalytic subunit of protein phosphatase-1 (PP1c). SMARCB1 has been reported to bind PP1c and to the PP1 regulatory subunit 15 (PPP1R15A/GADD34), and it was shown to increase PP1c activity in solution (35). Thus, a likely explanation for increased eIF2α phosphorylation in *SMARCB1* knockdown cells is diminished PP1c activity. Elevated eIF2α phosphorylation levels were also detected upon endoplasmic reticulum stress induction in human SMARCB1-negative in comparison with SMARCB1-positive tumor cell lines (Fig. 7C). Immunostainings revealed that SMARCB1 is not only present in the nucleus but also colocalized with the endoplasmic reticulum marker calnexin in the cytoplasm (Fig. 7D). Because phosphorylation of eIF2α is known to enhance apoptosis in combination with proteasome inhibition, we investigated this in cells with reduced or absent SMARCB1. Indeed, treatment with the proteasome inhibitor bortezomib resulted in increased apoptosis of MCF7-SMARCB1 knockdown cells, and of a kidney MRT and a brain AT/RT cell line, in comparison with *SMARCB1*-expressing control cells (Fig. 7E and F).

## Discussion

Our investigations revealed several important and novel aspects about the origin of different brain tumors, the role of genetic alterations in specifying tumor phenotypes, and the involvement of the UPR in tumors lacking SMARCB1.

We show that 3 brain tumor types can develop from the same pool of $p53^{-/-}$ postnatal murine NSC/NPCs and that their generation is directed by the type and order of genetic perturbations. The fact that all 3 are very aggressive and resemble human tumor types occurring in younger patients (the generated murine glioma is reminiscent of human giant cell glioblastoma) may be explained by the cell-of-origin: NSC/NPCs were derived from young (4-week-old) mice, and these cells have a higher proliferative potential than NPC/NPCs from older animals. GSEA revealed that the expression profiles of the 3 murine tumors correspond to respective human tumor signatures and the genes that directed the development of these murine tumors are also implicated in the pathogenesis of respective human tumor types. *TP53* is often inactivated in human high-grade gliomas (36, 37) and positive p53 staining is found in CNS PNETs and AT/RTs, indicating a stabilized p53 protein of altered functionality or an altered p53 pathway (38). *HRAS* mutations are not common in human gliomas, but increased copy numbers of *RAS/RAF* genes and increased RAS activity have been reported (36, 39). *MYC* and *MYCN* amplifications are a frequent feature of human CNS PNETs (40), and MYC is upregulated in human AT/RTs (41).

Classical human AT/RT is a very aggressive CNS tumor of infants and children. In the majority of cases, inactivation of the tumor suppressor gene *SMARCB1* is found (13). Although no evidence for loss-of-function of this gene was detected in our *HRAS*- and *MYC*-induced murine AT/RT-like tumors, we found that the gene expression pattern of these tumors showed other similarities with human AT/RTs and with mouse fibroblasts lacking *Smarcb1* (see below). These data suggest that different genetic events can also produce a similar tumor phenotype.

In addition to well-known phenotypic and genetic changes that occur during the progression of the same tumor type (from lower to higher grade tumors or benign to malignant lesions, such as the adenoma–carcinoma sequence; ref. 42), the coexistence or sequential appearance

of 2 distinct malignant tumors in the same tissue has been described. We show that an established *in vivo* tumor type (CNS PNET) can shift to another one (AT/RT-like tumor), and that this process is driven by the overexpression of a single gene. It was previously shown that the insertion of the v-Ha-*ras* gene into a small cell lung cancer cell line carrying an amplified *MYC* gene induces a transition to a large cell undifferentiated lung carcinoma *in vitro*, whereas no transition occurred when v-Ha-*ras* was inserted in small cell lung cancer cell lines without *MYC* amplification (43). We report that a single gene can trigger the transition of one *in vivo* tumor type to another. Previous studies have shown that the order of transcription factor gene expression directs the specification of normal hematopoietic cells (44) and that the relative order of *K-ras* and *APC* gene mutations determines the grade, but not the tumor type in case of lung neoplasia (45). With the reservation that our system is based on the strong expression of *MYC* and *HRAS* under the CMV promoter and includes an *ex vivo* step, we provide proof-of-principle that the order of genetic events can specify *in vivo* tumor types. It is conceivable that *MYC*-overexpressing tumors are particularly plastic and prone to phenotype transitions as *MYC* promotes cellular reprogramming into induced pluripotent stem cells with broad developmental potential (46). A possible explanation for the failure of *MYC* to turn *HRAS*-overexpressing glioma cells into AT/RT-like tumors is the inaccessibility of MYC-binding sites in the glioma cells, which might be required to regulate genes determining the AT/RT-like type. Taken together, we propose an additional parameter to influence the specification of tumor types: cell-of-origin, genetic and epigenetic events, and the order of genetic events.

Our results obtained in the second part of this study highlight that SMARCB1, a tumor suppressor primarily known for its role in chromatin remodeling, has another important function related to the UPR. This pathway serves as a cellular mechanism to cope with conditions leading to increased protein misfolding, such as hypoxia and nutrient deprivation in rapidly growing tumors. Activation of the UPR can have different consequences, either increased survival or cell death, which seems to depend on the different UPR branches and the dynamics of the response. The murine AT/RT-like tumors show an activation of the UPR according to their gene expression profile. Moreover, eosinophilic cytoplasmic inclusions, a feature of AT/RTs, are found in cells under endoplasmic reticulum stress (47) and in some of our AT/RT-like tumors. An activated UPR could result from reduced glucose availability due to the rapid growth of these tumorspheres or could be related to *MYC* and *HRAS* overexpression: MYC enhances protein translation, thus increasing the endoplasmic reticulum protein load, and the mutated form of *HRAS* used in our study (*V12 HRAS*) has been shown to particularly induce the UPR pathway (48). Our analysis of previously published gene expression profiles from human AT/RTs that lack *SMARCB1* and *Smarcb1*-deficient mouse embryonic fibroblasts (49) show the activation of many UPR-related genes. Most notably, our experimental results reveal that reduced levels of the SMARCB1 protein, which has previously only been shown to activate PP1c-GADD34 in solution (35), accounts for an elevated cellular sensitivity toward eIF2α phosphorylation, a central UPR mechanism. Sustained eIF2α phosphorylation confers cytoprotection against hypoxia, oxidative stress, and long-term glucose deficiency, all of which represent typical *in vivo* conditions of rapidly growing tumors (50–54). Importantly, we show that the application of the proteasome inhibitor bortezomib, which increases endoplasmic reticulum stress and synergizes with a chemical inhibitor of the GADD34-PP1c complex (55), enhances apoptosis of cells with reduced *SMARCB1* levels. Future studies should investigate whether such an approach could represent a novel targeted strategy for treating AT/RTs and related malignancies.

## Supplementary Material

Refer to Web version on PubMed Central for supplementary material.

## Acknowledgments

The authors thank Rogier Versteeg, Andreas Faissner, Rupert Handgretinger, Michael Grotzer, Matthias Simon, Angelika Tölle, and Peter Nilsson-Ehle for materials, Ann-Charlott Olsson, Irene Pala, and Ann-Sofie Albrecht for technical assistance.

**Grant Support**

The work was supported by Vetenskapsrådet (VR2007-2624, VR2007-4752), a Swedish public health grant, Barncancerfonden (BCF PROJ08/068), Cancerfonden (CAN2008/962), BayGene, NIH (C46274).

## References

1. Visvader JE. Cells of origin in cancer. Nature. 2011; 469:314–322. [PubMed: 21248838]
2. Gibson P, Tong Y, Robinson G, Thompson MC, Currle DS, Eden C, et al. Subtypes of medulloblastoma have distinct developmental origins. Nature. 2010; 468:1095–1099. [PubMed: 21150899]
3. Jacques TS, Swales A, Brzozowski MJ, Henriquez NV, Linehan JM, Mirzadeh Z, et al. Combinations of genetic mutations in the adult neural stem cell compartment determine brain tumour phenotypes. EMBO J. 2010; 29:222–235. [PubMed: 19927122]
4. Schuller U, Heine VM, Mao J, Kho AT, Dillon AK, Han YG, et al. Acquisition of granule neuron precursor identity is a critical determinant of progenitor cell competence to form Shh-induced medulloblastoma. Cancer Cell. 2008; 14:123–134. [PubMed: 18691547]
5. Yang ZJ, Ellis T, Markant SL, Read TA, Kessler JD, Bourboulas M, et al. Medulloblastoma can be initiated by deletion of Patched in lineage-restricted progenitors or stem cells. Cancer Cell. 2008; 14:135–145. [PubMed: 18691548]
6. Sutter R, Shakhova O, Bhagat H, Behesti H, Sutter C, Penkar S, et al. Cerebellar stem cells act as medulloblastoma-initiating cells in a mouse model and a neural stem cell signature characterizes a subset of human medulloblastomas. Oncogene. 2010; 29:1845–1856. [PubMed: 20062081]
7. Alcantara Llaguno S, Chen J, Kwon CH, Jackson EL, Li Y, Burns DK, et al. Malignant astrocytomas originate from neural stem/progenitor cells in a somatic tumor suppressor mouse model. Cancer Cell. 2009; 15:45–56. [PubMed: 19111880]
8. Bachoo RM, Maher EA, Ligon KL, Sharpless NE, Chan SS, You MJ, et al. Epidermal growth factor receptor and Ink4a/Arf: convergent mechanisms governing terminal differentiation and transformation along the neural stem cell to astrocyte axis. Cancer Cell. 2002; 1:269–277. [PubMed: 12086863]
9. Huse JT, Holland EC. Genetically engineered mouse models of brain cancer and the promise of preclinical testing. Brain Pathol. 2009; 19:132–143. [PubMed: 19076778]
10. Liu HK, Wang Y, Belz T, Bock D, Takacs A, Radlwimmer B, et al. The nuclear receptor tailless induces long-term neural stem cell expansion and brain tumor initiation. Genes Dev. 2010; 24:683–695. [PubMed: 20360385]
11. Wang Y, Yang J, Zheng H, Tomasek GJ, Zhang P, McKeever PE, et al. Expression of mutant p53 proteins implicates a lineage relationship between neural stem cells and malignant astrocytic glioma in a murine model. Cancer Cell. 2009; 15:514–526. [PubMed: 19477430]
12. Roberts CW, Orkin SH. The SWI/SNF complex–chromatin and cancer. Nat Rev Cancer. 2004; 4:133–142. [PubMed: 14964309]
13. Biegel JA, Zhou JY, Rorke LB, Stenstrom C, Wainwright LM, Fogelgren B. Germ-line and acquired mutations of INI1 in atypical teratoid and rhabdoid tumors. Cancer Res. 1999; 59:74–79. [PubMed: 9892189]
14. Hollmann TJ, Hornick JL. INI1-deficient tumors: diagnostic features and molecular genetics. Am J Surg Pathol. 2011; 35:e47–e63. [PubMed: 21934399]
15. Versteege I, Sevenet N, Lange J, Rousseau-Merck MF, Ambros P, Handgretinger R, et al. Truncating mutations of hSNF5/INI1 in aggressive paediatric cancer. Nature. 1998; 394:203–206. [PubMed: 9671307]

16. Subramanian A, Tamayo P, Mootha VK, Mukherjee S, Ebert BL, Gillette MA, et al. Gene set enrichment analysis: a knowledge-based approach for interpreting genome-wide expression profiles. Proc Natl Acad Sci U S A. 2005; 102:15545–15550. [PubMed: 16199517]
17. Garvin AJ, Re GG, Tarnowski BI, Hazen-Martin DJ, Sens DA. The G401 cell line, utilized for studies of chromosomal changes in Wilms' tumor, is derived from a rhabdoid tumor of the kidney. Am J Pathol. 1993; 142:375–380. [PubMed: 8382007]
18. Bracken AP, Pasini D, Capra M, Prosperini E, Colli E, Helin K. EZH2 is downstream of the pRB-E2F pathway, essential for proliferation and amplified in cancer. EMBO J. 2003; 22:5323–5335. [PubMed: 14532106]
19. Ding H, Roncari L, Shannon P, Wu X, Lau N, Karaskova J, et al. Astrocyte-specific expression of activated p21-ras results in malignant astrocytoma formation in a transgenic mouse model of human gliomas. Cancer Res. 2001; 61:3826–3836. [PubMed: 11325859]
20. Herms JW, von Loewenich FD, Behnke J, Markakis E, Kretzschmar HA. c-myc oncogene family expression in glioblastoma and survival. Surg Neurol. 1999; 51:536–542. [PubMed: 10321885]
21. Leung C, Lingbeek M, Shakhova O, Liu J, Tanger E, Saremaslani P, et al. Bmi1 is essential for cerebellar development and is overexpressed in human medulloblastomas. Nature. 2004; 428:337–341. [PubMed: 15029199]
22. Liu M, Dai B, Kang SH, Ban K, Huang FJ, Lang FF, et al. FoxM1B is overexpressed in human glioblastomas and critically regulates the tumorigenicity of glioma cells. Cancer Res. 2006; 66:3593–3602. [PubMed: 16585184]
23. Rajasekhar VK, Begemann M. Concise review: roles of polycomb group proteins in development and disease: a stem cell perspective. Stem Cells. 2007; 25:2498–2510. [PubMed: 17600113]
24. Martina E, Degen M, Ruegg C, Merlo A, Lino MM, Chiquet-Ehrismann R, et al. Tenascin-W is a specific marker of glioma-associated blood vessels and stimulates angiogenesis *in vitro*. FASEB J. 2010; 24:778–787. [PubMed: 19884327]
25. Hirata E, Arakawa Y, Shirahata M, Yamaguchi M, Kishi Y, Okada T, et al. Endogenous tenascin-C enhances glioblastoma invasion with reactive change of surrounding brain tissue. Cancer Sci. 2009; 100:1451–1459. [PubMed: 19459858]
26. Restrepo A, Smith CA, Agnihotri S, Shekarforoush M, Kongkham PN, Seol HJ, et al. Epigenetic regulation of glial fibrillary acidic protein by DNA methylation in human malignant gliomas. Neuro Oncol. 2011; 13:42–50. [PubMed: 21075782]
27. Tibshirani R, Hastie T, Narasimhan B, Chu G. Diagnosis of multiple cancer types by shrunken centroids of gene expression. Proc Natl Acad Sci U S A. 2002; 99:6567–6572. [PubMed: 12011421]
28. Kao CL, Chiou SH, Ho DM, Chen YJ, Liu RS, Lo CW, et al. Elevation of plasma and cerebrospinal fluid osteopontin levels in patients with atypical teratoid/rhabdoid tumor. Am J Clin Pathol. 2005; 123:297–304. [PubMed: 15842057]
29. Toy H, Yavas O, Eren O, Genc M, Yavas C. Correlation between osteopontin protein expression and histological grade of astrocytomas. Pathol Oncol Res. 2009; 15:203–207. [PubMed: 19048398]
30. Frazer KA, Pachter L, Poliakov A, Rubin EM, Dubchak I. VISTA: computational tools for comparative genomics. Nucleic Acids Res. 2004; 32:W273–W279. [PubMed: 15215394]
31. Motohashi H, Yamamoto M. Nrf2-Keap1 defines a physiologically important stress response mechanism. Trends Mol Med. 2004; 10:549–557. [PubMed: 15519281]
32. Healy SJ, Gorman AM, Mousavi-Shafaei P, Gupta S, Samali A. Targeting the endoplasmic reticulum-stress response as an anticancer strategy. Eur J Pharmacol. 2009; 625:234–246. [PubMed: 19835867]
33. Isakoff MS, Sansam CG, Tamayo P, Subramanian A, Evans JA, Fillmore CM, et al. Inactivation of the Snf5 tumor suppressor stimulates cell cycle progression and cooperates with p53 loss in oncogenic transformation. Proc Natl Acad Sci U S A. 2005; 102:17745–17750. [PubMed: 16301525]
34. Xu Y, Yan W, Chen X. SNF5, a core component of the SWI/SNF complex, is necessary for p53 expression and cell survival, in part through eIF4E. Oncogene. 2010; 29:4090–4100. [PubMed: 20473326]

35. Wu DY, Tkachuck DC, Roberson RS, Schubach WH. The human SNF5/INI1 protein facilitates the function of the growth arrest and DNA damage-inducible protein (GADD34) and modulates GADD34-bound protein phosphatase-1 activity. J Biol Chem. 2002; 277:27706–27715. [PubMed: 12016208]
36. The Cancer Genome Atlas Research Network. Comprehensive genomic characterization defines human glioblastoma genes and core pathways. Nature. 2008; 455:1061–1068. [PubMed: 18772890]
37. Parsons DW, Jones S, Zhang X, Lin JC, Leary RJ, Angenendt P, et al. An integrated genomic analysis of human glioblastoma multiforme. Science. 2008; 321:1807–1812. [PubMed: 18772396]
38. Eberhart CG, Chaudhry A, Daniel RW, Khaki L, Shah KV, Gravitt PE. Increased p53 immunopositivity in anaplastic medulloblastoma and supratentorial PNET is not caused by JC virus. BMC Cancer. 2005; 5:19. [PubMed: 15717928]
39. Jeuken J, van den Broecke C, Gijsen S, Boots-Sprenger S, Wesseling P. RAS/RAF pathway activation in gliomas: the result of copy number gains rather than activating mutations. Acta Neuropathol. 2007; 114:121–133. [PubMed: 17588166]
40. Behdad A, Perry A. Central nervous system primitive neuroectodermal tumors: a clinicopathologic and genetic study of 33 cases. Brain Pathol. 2010; 20:441–450. [PubMed: 19725831]
41. Ma HI, Kao CL, Lee YY, Chiou GY, Tai LK, Lu KH, et al. Differential expression profiling between atypical teratoid/rhabdoid and medulloblastoma tumor *in vitro* and *in vivo* using microarray analysis. Childs Nerv Syst. 2010; 26:293–303. [PubMed: 19902219]
42. Fearon ER, Vogelstein B. A genetic model for colorectal tumorigenesis. Cell. 1990; 61:759–767. [PubMed: 2188735]
43. Mabry M, Nakagawa T, Nelkin BD, McDowell E, Gesell M, Eggleston JC, et al. v-Ha-ras oncogene insertion: a model for tumor progression of human small cell lung cancer. Proc Natl Acad Sci U S A. 1988; 85:6523–6527. [PubMed: 2842776]
44. Iwasaki H, Mizuno S, Arinobu Y, Ozawa H, Mori Y, Shigematsu H, et al. The order of expression of transcription factors directs hierarchical specification of hematopoietic lineages. Genes Dev. 2006; 20:3010–3021. [PubMed: 17079688]
45. Johnson L, Mercer K, Greenbaum D, Bronson RT, Crowley D, Tuveson DA, et al. Somatic activation of the K-ras oncogene causes early onset lung cancer in mice. Nature. 2001; 410:1111–1116. [PubMed: 11323676]
46. Nakagawa M, Takizawa N, Narita M, Ichisaka T, Yamanaka S. Promotion of direct reprogramming by transformation-deficient Myc. Proc Natl Acad Sci U S A. 2010; 107:14152–14157. [PubMed: 20660764]
47. Yamagishi S, Koyama Y, Katayama T, Taniguchi M, Hitomi J, Kato M, et al. An *in vitro* model for Lewy body-like hyaline inclusion/astrocytic hyaline inclusion: induction by ER stress with an ALS-linked SOD1 mutation. PLoS One. 2007; 2:e1030. [PubMed: 17925878]
48. Denoyelle C, Abou-Rjaily G, Bezrookove V, Verhaegen M, Johnson TM, Fullen DR, et al. Anti-oncogenic role of the endoplasmic reticulum differentially activated by mutations in the MAPK pathway. Nat Cell Biol. 2006; 8:1053–1063. [PubMed: 16964246]
49. Pomeroy SL, Tamayo P, Gaasenbeek M, Sturla LM, Angelo M, McLaughlin ME, et al. Prediction of central nervous system embryonal tumour outcome based on gene expression. Nature. 2002; 415:436–442. [PubMed: 11807556]
50. Bi M, Naczki C, Koritzinsky M, Fels D, Blais J, Hu N, et al. ER stress-regulated translation increases tolerance to extreme hypoxia and promotes tumor growth. EMBO J. 2005; 24:3470–3481. [PubMed: 16148948]
51. Harding HP, Zhang Y, Zeng H, Novoa I, Lu PD, Calfon M, et al. An integrated stress response regulates amino acid metabolism and resistance to oxidative stress. Mol Cell. 2003; 11:619–633. [PubMed: 12667446]
52. Koumenis C, Naczki C, Koritzinsky M, Rastani S, Diehl A, Sonenberg N, et al. Regulation of protein synthesis by hypoxia via activation of the endoplasmic reticulum kinase PERK and phosphorylation of the translation initiation factor eIF2alpha. Mol Cell Biol. 2002; 22:7405–7416. [PubMed: 12370288]

53. Muaddi H, Majumder M, Peidis P, Papadakis AI, Holcik M, Scheuner D, et al. Phosphorylation of eIF2alpha at serine 51 is an important determinant of cell survival and adaptation to glucose deficiency. Mol Biol Cell. 2010; 21:3220–3231. [PubMed: 20660158]

54. Wiseman RL, Balch WE. A new pharmacology–drugging stressed folding pathways. Trends Mol Med. 2005; 11:347–350. [PubMed: 16005683]

55. Schewe DM, Aguirre-Ghiso JA. Inhibition of eIF2alpha dephosphorylation maximizes bortezomib efficiency and eliminates quiescent multiple myeloma cells surviving proteasome inhibitor therapy. Cancer Res. 2009; 69:1545–1552. [PubMed: 19190324]

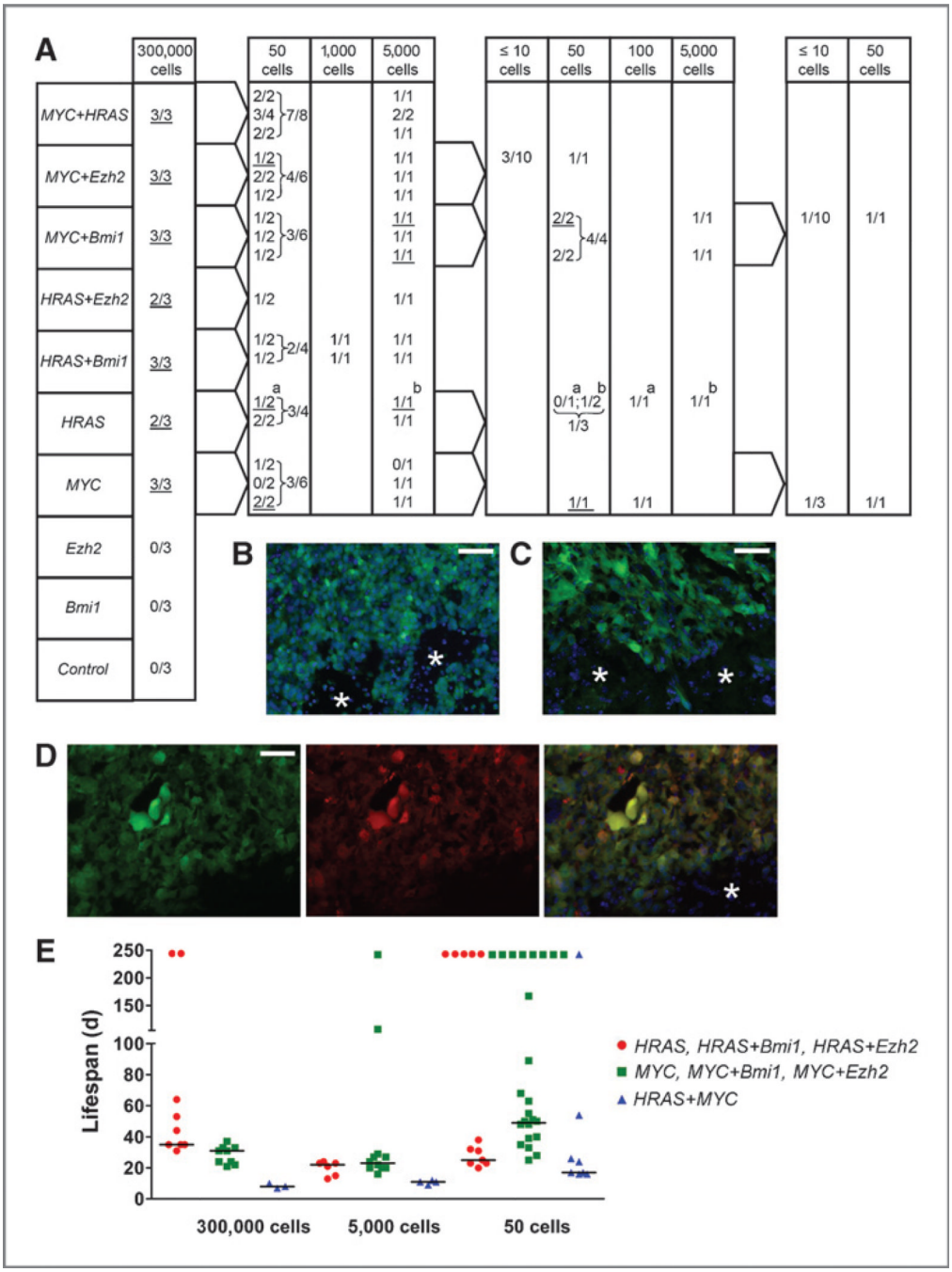


**Figure 1.**

Serial intracranial transplantations of p53$^{-/-}$ NSC/NPCs expressing different genes (*MYC*, *HRAS*, *Bmi1*, and *Ezh2*) and of eGFP control cells. A, primary to quaternary transplantations from left to right. The number of mice with tumors/number of transplanted mice is shown. Cells from underlined tumors were FACS isolated and used in subsequent transplantations. For example, 3 of 3 mice transplanted with 300,000 *MYC* overexpressing cells developed tumors. A total of 50 cells from each of the 3 tumors were transplanted into 2 recipient mice and 5,000 cells from each tumor into one animal. Both animals that received 50 cells from the third primary tumor developed tumors, and cells from one of these 50 cell tumors (underlined) were further transplanted into tertiary recipients: one

animal received 50 and another 100 cells. Both animals developed tumors, and cells from the first one (underlined) were used in quarternary transplantations (3 mice receiving 10 cells or less and one animal receiving 50 cells). In all cases, except for the one in which tumors are marked with a and b, only one tumor sample of each genetic type was used for subsequent transplantations. Cryosections of secondary tumors from cells overexpressing *MYC* (B), *HRAS* (C), and *MYC* together with *HRAS* (D) showing green (B, C) or green and red fluorescent tumor cells (D). Asterisk, adjacent normal tissue; scale bars, 50 μm. E, life span of tumor-bearing mice (in days) from primary to quaternary transplantations. Tumors are grouped according to their histology: gliomas (red dots),CNSPNETs (green squares), AT/RT-like (blue triangles). Horizontal lines: median lifespan values of animals that developed tumors (from left to right: 35,31,8/22,23,11/25,49,17). Animals that were alive after 244 days were not included in the calculation and are indicated on top.

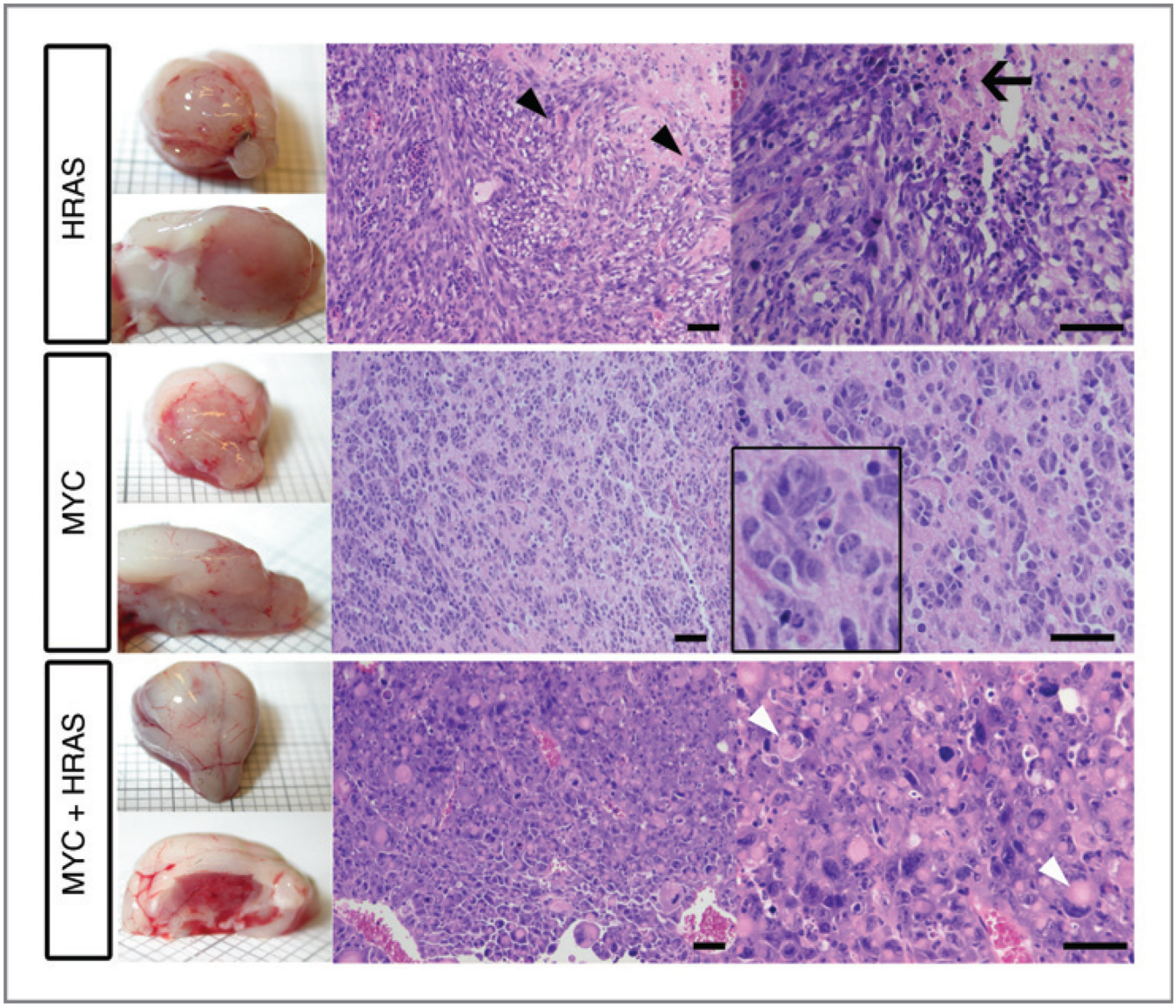


**Figure 2.**

Images of brain tumors that developed upon transplantation of $p53^{-/-}$ NSC/NPCs overexpressing *HRAS*, *MYC*, and *HRAS* together with *MYC*. Hematoxylin/eosin-stained paraffin sections. *HRAS*-overexpressing tumors show high-grade glioma features with abundant spindle-formed cells, necrosis (arrow), and single giant cells containing pleomorphic and/or multiple nuclei (black arrow heads). Tumors with PNET features (developed upon *MYC* overexpression) consist of small round cells with a large nuclear to cytoplasmic ratio, sometimes forming rosette-like structures (magnified section). Tumors derived from NSC/NPCs overexpressing *MYC* together with *HRAS* show AT/RT-like features. They consist of a large number of rhabdoid cells with eccentric nuclei and prominent nucleoli. Many cells have eosinophilic cytoplasmic inclusions (white arrow head). In addition, smaller cells with scant cytoplasm displaying PNET features are present. Scale bars, 50 μm.

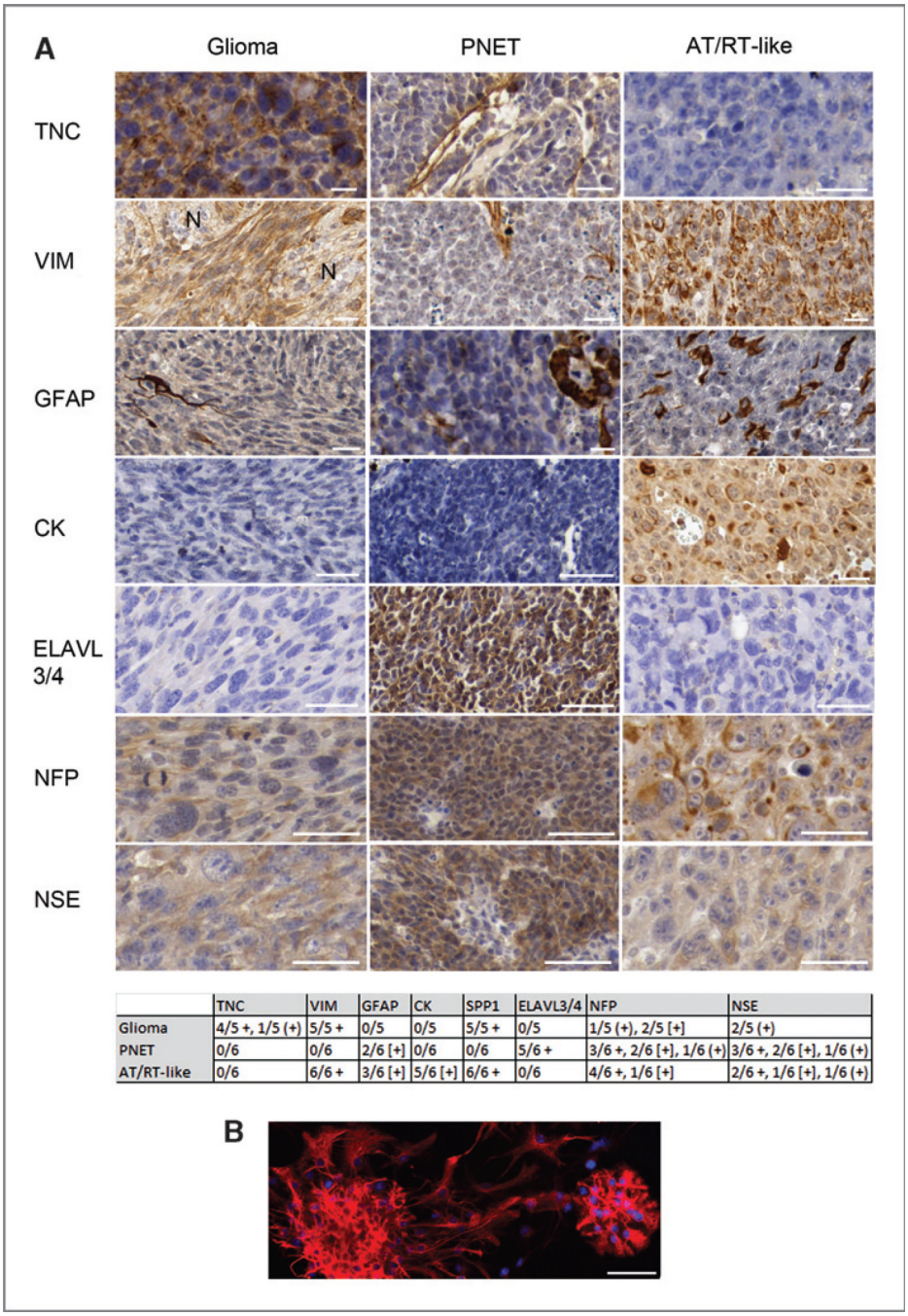


| | TNC | VIM | GFAP | CK | SPP1 | ELAVL3/4 | NFP | NSE |
|---|---|---|---|---|---|---|---|---|
| Glioma | 4/5 +, 1/5 (+) | 5/5 + | 0/5 | 0/5 | 5/5 + | 0/5 | 1/5 (+), 2/5 [+] | 2/5 (+) |
| PNET | 0/6 | 0/6 | 2/6 [+] | 0/6 | 0/6 | 5/6 + | 3/6 +, 2/6 [+], 1/6 (+) | 3/6 +, 2/6 [+], 1/6 (+) |
| AT/RT-like | 0/6 | 6/6 + | 3/6 [+] | 5/6 [+] | 6/6 + | 0/6 | 4/6 +, 1/6 [+] | 2/6 +, 1/6 [+], 1/6 (+) |

**Figure 3.**

A, immunohistochemistry of tumors and B, GFAP-staining (red) of p53-deficient neurospheres. Blue staining in B: 4′, 6-diamidino-2-phenylindole–positive nuclei. Paraffin-embedded sections stained with antibodies against tenascin-C (TNC), vimentin (VIM), GFAP, cytokeratin (CK), ELAVL3/4, neurofilament (NFP), and neuron-specific enolase (NSE). Protein staining: brown, counterstaining: blue. The table summarizes all immunohistochemistry results. +, staining of the majority of tumor cells; (+), weak staining; [+], staining of a few tumor cells. N, adjacent normal brain. In CNS PNET, the vimentin antibody stains blood vessels and reactive glia, and the tenascin-C antibody shows blood vessel-associated staining. Scale bars, 50 μm.

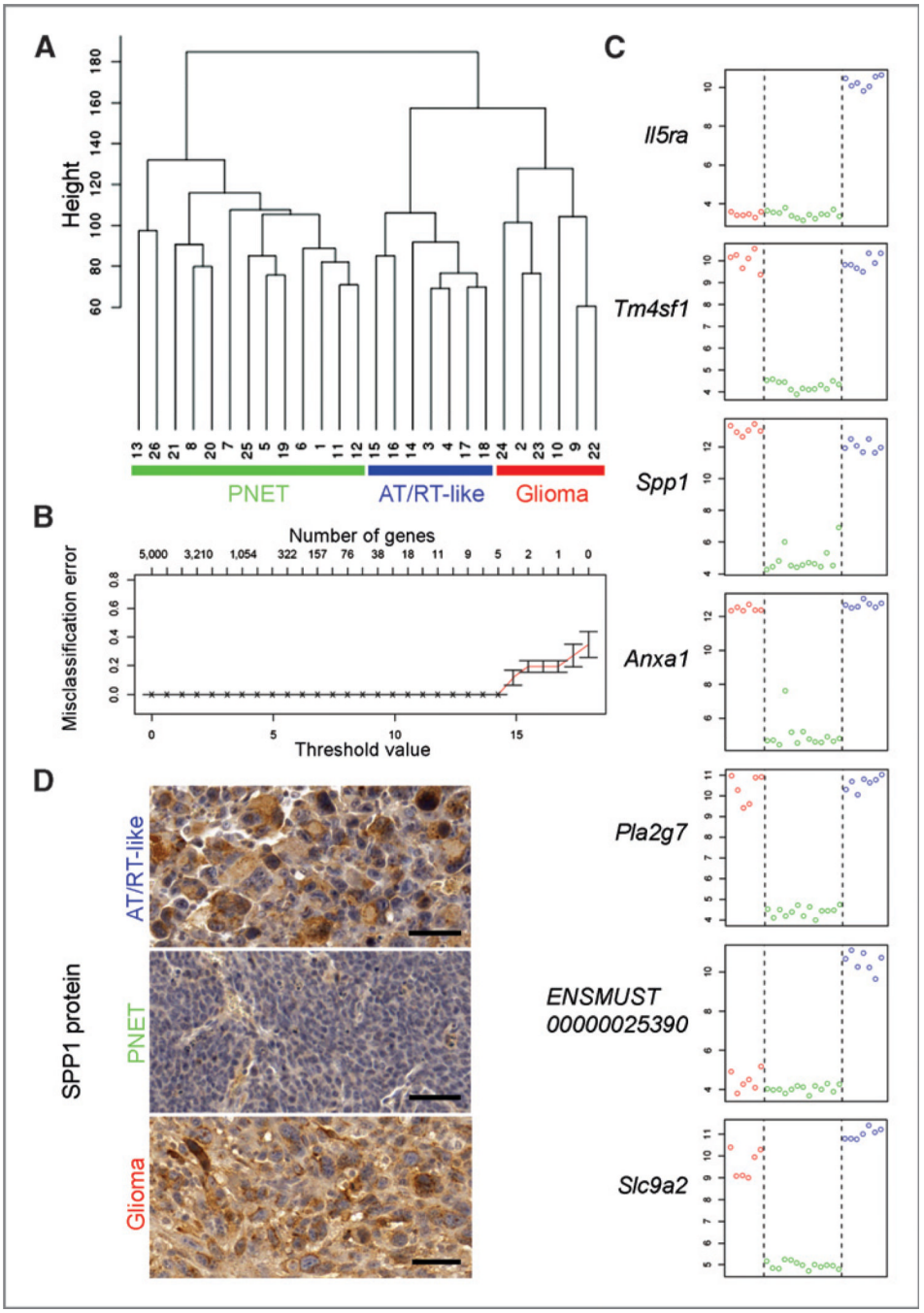


**Figure 4.**

Gene expression analyses of brain tumor cells. A,unsupervised clustering of FACS-isolated tumorsphere cells from 26 tumors based on microarray data. Y-axis: Euclidean distance. Three major clusters are identified based on the 5,000 most variable genes. They correspond to the 3 histologic tumor types. Internal array sample numbers are shown (Supplementary Table S1). B, prediction analysis using the 5,000 most variable genes over all 26 samples. Different threshold values corresponding to different numbers of genes are shown along the X-axis. A classification into the 3 tumor types can be done, with minimal cross-validation error and considering the risk of overfitting, based on the expression information of a minimum of 7 genes. C, relative expression values of the 7 genes that allows for

classification of the 3 tumor types (y-axis) plotted against the 26 tumorsphere samples (x-axis). Red circles (left side): glioma samples, green circles (middle section): CNS PNET samples, blue circles (right side): AT/RT-like samples. D, confirmation of the differential expression of *Spp1* by immunohistochemistry. In CNS PNET tumors, SPP1 staining is confined to blood vessels and immune cells, and virtually absent in tumor cells. Scale bars: 50 μm.

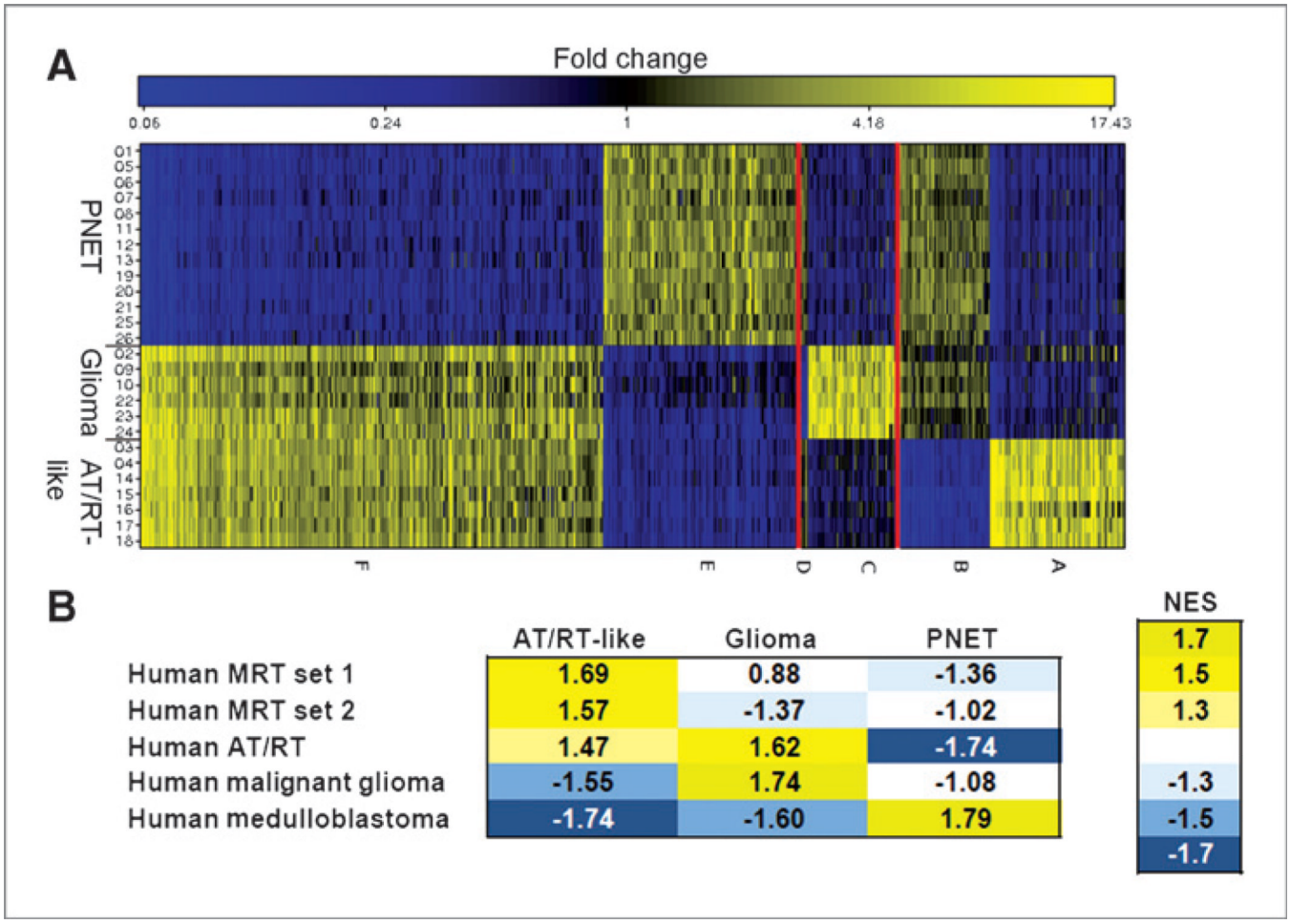


**Figure 5.**

Gene groups representing the 3 different tumor types. A, color coded relative gene expression differences of the 1,000 genes with maximum expression correlation to the 3 tumor types: Higher (yellow) and lower (blue) expression levels. Genes are plotted along the x-axis, tumor types along the y-axis. Six groups of genes were identified (A–F) with the highest correlation to one of the 3 tumor types. B, GSEA. A color-coded heatmap showing the enrichment of human brain tumor gene sets in the comparative gene expression data of the respective murine tumor types is depicted. Each tumor type was analyzed in comparison with the other two. The NES and color code indicate the degree of enrichment. High positive NES, confirming an enrichment, are shown in yellow; negative NES (blue) indicate that the human gene set is not enriched in the analyzed murine tumor type, but rather in the control group (i.e., the respective other 2 murine tumor types). Gene sets are listed in Supplementary File S1.

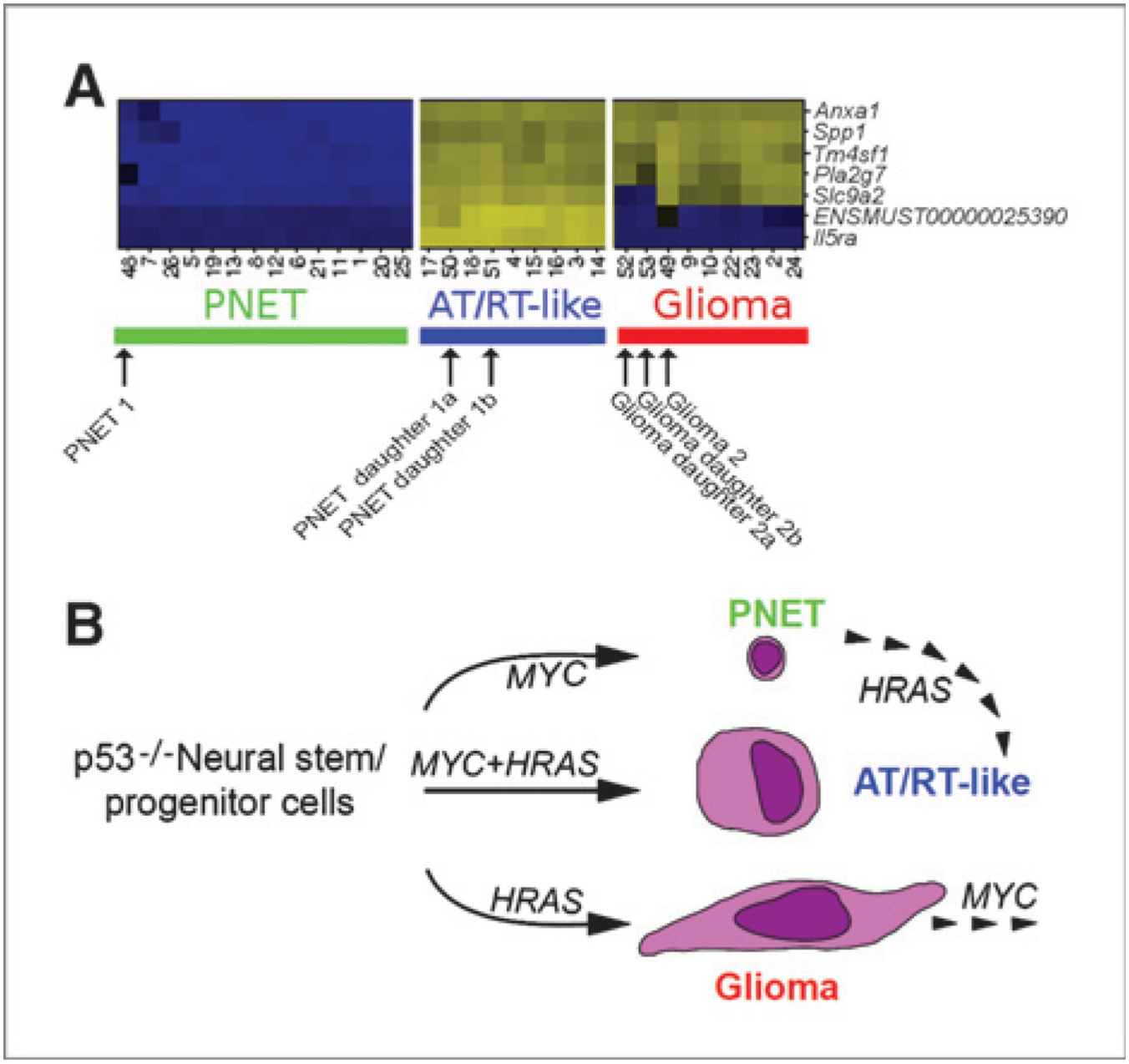


**Figure 6.**

Microarray data analysis and summary of consecutive perturbation experiments. A, heatmap of the expression data used in tumor classification. Columns: tumorsphere cells from 26 tumors (developed after primary to tertiary transplantations) together with cells from one CNS PNET and one glioma mother tumor and respective daughter tumors (developed upon consecutive perturbations). Rows: 7 signature genes that allow for a classification of the 3 tumor types. Relative gene expression is color coded (higher expression: yellow, lower expression: blue). Internal array sample numbers are shown (Supplementary Table S1). B, schematic summary of the consecutive perturbation experiments.

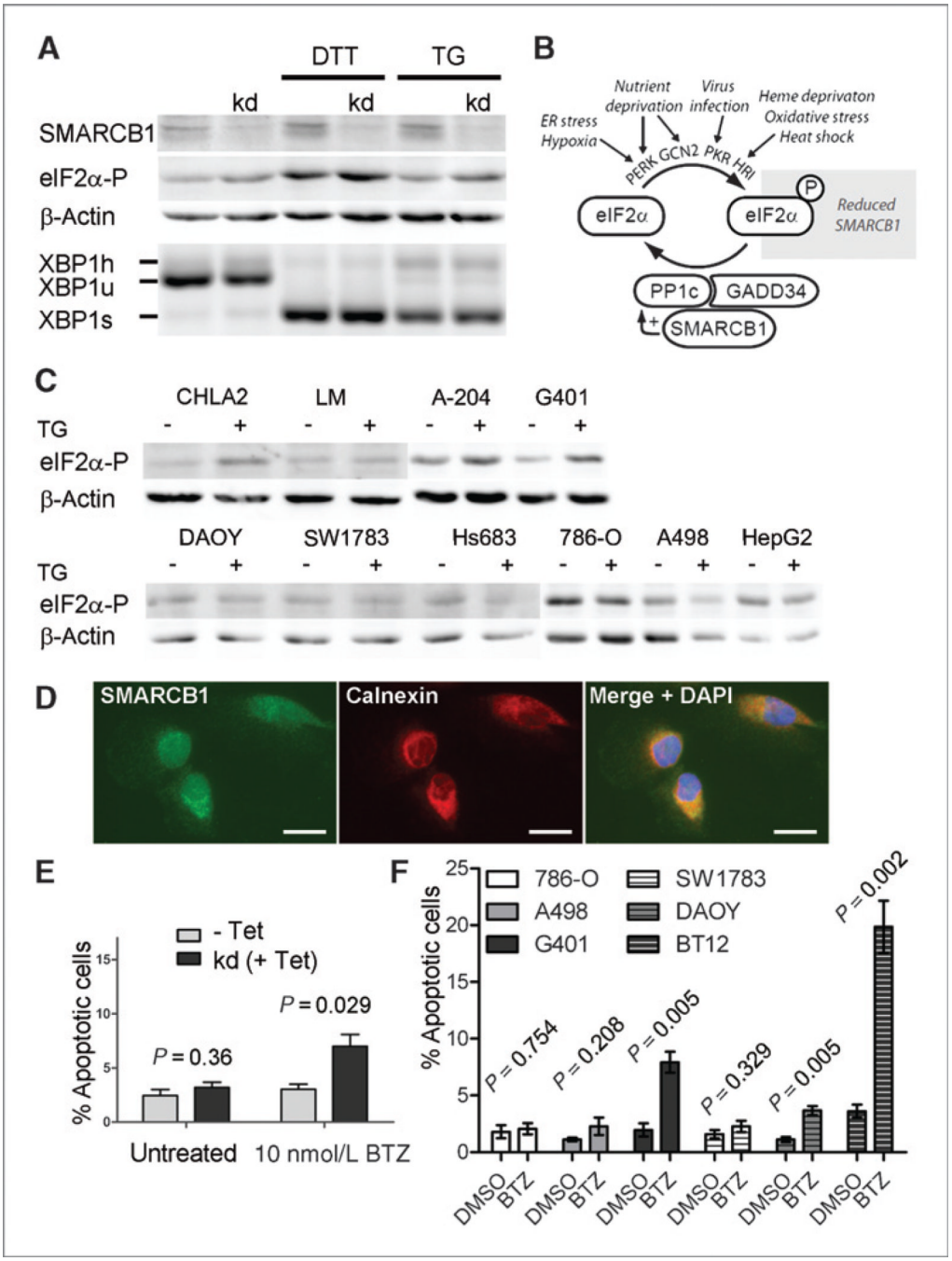


**Figure 7.**

Involvement of SMARCB1 in the UPR. A, shRNA-mediated SMARCB1 knockdown in MCF7 cells (tetracycline induced) leads to increased eIF2α phosphorylation as determined by immunoblots. Endoplasmic reticulum stress was induced by DTT and thapsigargin treatment for 3 hours. Unconventional splicing of XBP1 is shown by reverse transcriptase PCR as an indicator of another activated UPR branch. XBP1s, XBP1u, XBP1h: spliced, unspliced, and hybrid XBP1 cDNA (XBP1s/XBP1u heterodimers). B, schematic summary showing the connection between SMARCB1 and eIF2α phosphorylation. C, increased eIF2α phosphorylation levels upon 3-hour TG exposure are detected in the human AT/RT cell line CHLA2 and the human MRT cell lines LM (liver origin), A-204 (muscle origin),

and G401 (kidney origin), all of which lack SMARCB1, in comparison with human SMARCB1-positive brain tumor (DAOY, SW1783, Hs683), renal cell carcinoma (786-O, A-498) and hepatocellular carcinoma (HepG2) cell lines. Fold-change of β-actin–normalized phosphorylated eIF2α signal intensities between TG-treated and untreated cells: CHLA2: 5.89; LM: 1.27; A-204: 1.39; G401: 2.49; DAOY: 0.77; SW1783: 0.75; Hs683: 0.81; 786-O: 0.60; A-498: 1.12; HepG2: 0.56. D, SMARCB1 is present in the nucleus of 786-O cells and colocalizes with the endoplasmic reticulum marker calnexin in the cytoplasm. E, treatment of MCF7 cells with the proteasome inhibitor bortezomib for 12 hours leads to increased apoptosis in tetracycline (Tet)-induced SMARCB1 knockdown (kd) cells. Percentages of Annexin V–positive and 7AAD-negative apoptotic cells of 3 independent experiments are shown. Error bars: SEM. *P* values (unpaired *t* tests) comparing noninduced to Tet-induced cells. F, treatment of SMARCB1-positive renal cell carcinoma (786-O, A-498) and brain tumor (SW1783, DAOY) cells, a kidney MRT (G401), and a brain AT/RT cell line (BT12) cell line with 10 nmol/L bortezomib for 24 hours leads to highest apoptosis in the rhabdoid tumor cells G401 and BT12 compared with DMSO (dimethyl sulfoxide; vehicle)-treated cells. The kidney and brain tumor lines were kept under comparable adherent culture conditions, respectively. Percentages of Annexin V–positive and 7AAD-negative apoptotic cells of 3 independent experiments are shown. Error bars: SEM. *P* values (unpaired *t* tests) comparing bortezomib to DMSO-treated cells. BTZ, bortezomib; TG, thapsigargin.